Ionics (2021) 27:3365–3372
https://doi.org/10.1007/s11581-021-04098-7

ORIGINAL PAPER

Fabrication of hollow TiO_2 nanospheres for high-capacity and long-life lithium storage

Mengzhao Ding[1] · Lijie Cao[1] · Xuelong Miao[1] · Tian Sang[2] · Chaomin Zhang[2] · Yunxia Ping[2]

Received: 16 March 2021 / Revised: 10 May 2021 / Accepted: 12 May 2021 / Published online: 25 May 2021

Abstract

Titanium dioxide (TiO_2) is of great interest as anode material for lithium-ion batteries (LIBs) because of its safety, structure stability, and low cost. However, the limitations of low conductivity and small theoretical capacity prevent its further applications. Herein, TiO_2 nanospheres with a hollow structure (H-TiO_2) were successfully synthesized via a hard-template method. The resultant material used as LIBs anode with superior lithium storage properties in terms of high initial capacity (~289 mA h g^{-1} at 0.1 A g^{-1}), good rate capability (~101 mA h g^{-1} at 2 A g^{-1}), and excellent cycling stability (~196 mA h g^{-1} was retained over 300 cycles at 0.1 A g^{-1}). The improved performances are attributed to the large specific area (~225 m^2 g^{-1}) and abundant mesoporous of the hollow structure, which can not only promote the diffusion of Li^+ and e^- but also achieve an increase in the contact area between electrodes and electrolyte.

Keywords TiO_2 · Hard-template method · Hollow structure · Mesoporous · Lithium storage

Introduction

Various energy storage devices have been developed to solve the growing energy problem, such as supercapacitors, solar cells, and sodium-ion batteries. Among them, lithium-ion batteries are dominating the market due to their high-energy density, high cycle life, and eco-friendliness [1–5]. Titanium-based materials are regarded as promising anode materials in LIBs, among which titanium dioxide has drawn intensive interest because of its low cost, non-toxicity, and small volume change (< 4%) [6–8]. More importantly, titanium dioxide is highly safe as anode for LIBs owning to is electrochemically stable during Li^+ insertion/extraction processes and can avoid the occurrence of lithium electroplating [9, 10]. Nevertheless, the practical application of TiO_2 in LIBs has been severely hindered by poor electronic conductivity and low theoretical capacity [11, 12].

Fortunately, it has been demonstrated by many previous studies that nanostructured materials possess better lithium insertion/extraction kinetics and higher lithium storage capacity, improving the electrochemical performance by reducing the particle size of the electrode materials, has become a research hotspot [13–15]. In addition, constructing the hollow structure TiO_2 materials has also been proposed to enhance the lithium storage performance. As is known, hollow structures exhibit large specific area and abundant pores, which can efficiently enhance the electrochemical properties of electrode including specific capacity, rate capability, and cycling stability [16, 17]. For example, Tian et al. [18] designed the TiO_2 hollow nanowires with the diameter of 70 nm via chemical method followed by the calcination in a muffle furnace. The material shows the discharge capacity of 180 mA h g^{-1} at the current density of 0.2 C after 50 cycles. Gao et al. [19] prepared TiO_2 microboxes by template-free method, and the obtained material exhibits rate performance with the discharge capacity of 150 mA h g^{-1} at the current density of 2 C.

In this work, TiO_2 hollow nanospheres were successfully fabricated by a hard-template method. Compared with the solid TiO_2 nanoparticles, it is suggested that the as-prepared H-TiO_2 has unique advantages. (1) The large specific area of the H-TiO_2 can not only provide more active sites for lithium storage but also keep an increased contact area between the electrodes and the electrolyte. (2) The hollow structure with

✉ Lijie Cao
jqlx@sues.edu.cn

[1] School of Mechanical and Automotive Engineering, Shanghai University of Engineering Science, Shanghai 201620, China

[2] School of Mathematics, Physics and Statistics, Shanghai University of Engineering Science, Shanghai 201620, China

abundant mesoporous of the H-TiO_2 can efficiently promote transport rate of Li^+ and e^- in the electrodes. As expected, the HNS TiO_2 used as anode materials for LIBs exhibit superior rate ability with a capacity of 101 mA h g^{-1} at a current density of 2 A g^{-1} and an admirable discharge capacity of 196 mA h g^{-1} at a current density of 0.1 A g^{-1} after 300 cycles.

Experimental sections

Synthesis of H-TiO_2

A total of 5.8 ml of 28% ammonia solution and 2 ml of deionized water were added into 60 ml of ethanol under magnetic stirring, and then 4 ml of tetraethyl orthosilicate (TEOS) dispersed in 20 ml of ethanol was mixed into this solution. After stirring for 5 h, the white precipitate (SiO_2) was obtained by centrifugation and washed three times with deionized water and ethanol, respectively. Then, the collected precipitate was redispersed in 35 ml of ethanol, followed by the addition 0.1 g of hydroxypropyl cellulose (HPC) and 0.5 ml deionized water. Next, 1.2 ml of titanium butoxide (TBOT) dissolved in 15 ml of ethanol was injected into above solution and reacted at 80 °C for 2.5 h. The resulting precipitate (TiO_2@SiO_2) was collected by centrifugation and washed three times with deionized water and ethanol, respectively. After that, the precipitate was calcined under argon gas atmosphere, and then the calcined powder was added into 15 ml of 0.1 M NaOH solution stirring for 3 h. Finally, the H-TiO_2 were obtained by centrifugation and washed three times with deionized water and ethanol, respectively.

Synthesis of TiO_2 nanoparticles

For comparison, TiO_2 nanoparticles (N-TiO_2) were also prepared; 2 ml TBOT was mixed with 60 ml acetone stirring for 0.5 h at room temperature and then transferred to a PTFE-lined reaction kettle and reacted at 200 °C for 2 h. Next, the white precipitate (TiO_2) was obtained by centrifugation and washed three times with deionized water and acetone, respectively, followed by dried at 60 °C for 12 h and calcined at 600 °C for 3 h.

Materials characterization

The morphology and microstructural were analyzed with the scanning electron microscopy (SEM, Hitachi S4800) and transmission electron microscope (TEM, Tecnai-G2-F30 FEI with image corrector). The composition and crystal structure were characterized by X-ray diffraction (XRD, Rigaku, D/max-Rbusing Cu Ka radiation) measurement. The N_2 adsorption/desorption isotherms were measured with Micromeritics ASAP 2010 instrument.

Electrochemical measurements

Electrochemical tests were performed using CR2032-type coin cells. The working electrodes were prepared by mixing the active materials, acetylene black, and polyvinylidene fluoride (PVDF) with a weight ratio of 7:2:1 in N-methyl-2-pyrrolidone (NMP) to form a slurry. The slurry was uniformly spread on a copper foil. Pure lithium foil was used as the counter electrode. Celgard2400 was used as separator. A 1 M solution of $LiPF_6$ dissolved in ethylene carbonate and dimethyl carbonate (1:1 in volume ratio) was used as the electrolyte. The lithium half-cells were assembled in an argon-filled glovebox with both water and oxygen contents below 0.1 ppm. Cyclic voltammetry (CV) data were recorded using a PGSTAT302N electrochemical workstation. Galvanostatic discharge-charge curves were collected on a Neware battery test system within a voltage range of 1–3 V (vs Li^+/Li). Electrochemical impedance spectra (EIS) were also carried out on a PGSTAT302N electrochemical workstation in the frequency range of 0.1 Hz–100 kHz.

Results and discussion

A brief schematic diagram of the preparation process of H-TiO_2 is shown in Fig. 1a. The as-prepared uniformly sized SiO_2 was used as template to synthesize the TiO_2@SiO_2 precursor, which was then etched with NaOH solution to remove the SiO_2, resulting in H-TiO_2, and the detailed growth mechanism of H-TiO_2 as shown in supplementary information (SI). Fig. 2b shows the SEM image of the H-TiO_2. It can be clearly seen that these samples exhibit spherical structure with a uniform diameter of ~200 nm. Interestingly, several broken spheres can be observed, which reveals the hollow structure of the obtained TiO_2 materials. Their hollow interiors are further elucidated by TEM. Fig. 3c reveals a clear inner cavity by obvious comparison of the hollow inner cavity and the hollow outer cavity, which indicating that TiO_2@SiO_2 precursor were completely converted into TiO_2 hollow spherical structure, and the thickness of the H-TiO_2 shell is about 15 nm. The HRTEM image of the H-TiO_2 is also provided in Fig. 3d, a clear lattice with an interlayer spacing of 0.35 nm can be observed, which coinciding well with the (101) crystal planes of anatase TiO_2. The phase purity and crystalline structure of the H-TiO_2 were tested by X-ray diffraction (XRD) measurement, and the corresponding XRD pattern as shown in Fig. 2c. As can be seen, all the intensive diffraction peaks were well assigned to anatase TiO_2 (JCPDS no.21-1272) [20, 21]. And no peaks were observed for the other phases, indicating their high purity. Nitrogen adsorption-desorption measurements were used to investigate the specific surface area and pore size distribution of the H-TiO_2. The N_2 adsorption/desorption isotherms in Fig. 2d depict typical Type IV curves,

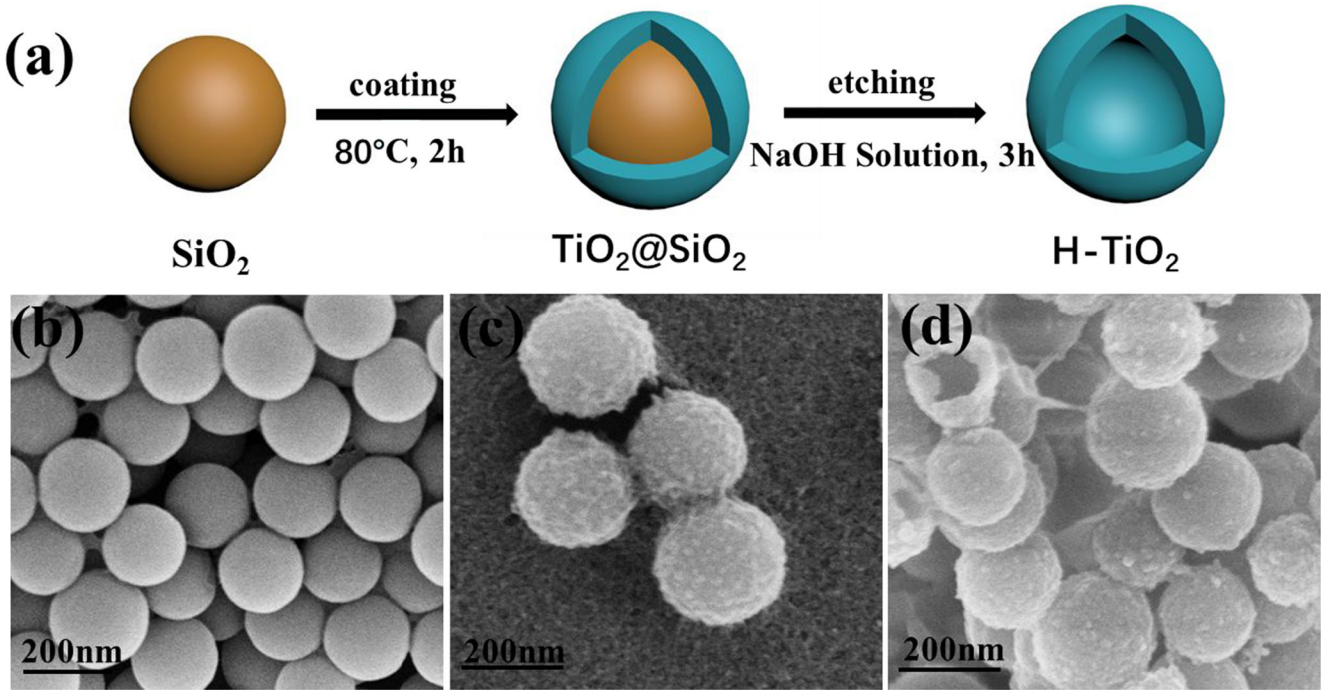

Fig. 1 **a** Schematic illustrations of synthesized process of H-TiO_2; SEM images of **b** SiO_2, **c** TiO_2@SiO_2, and **d** H-TiO_2

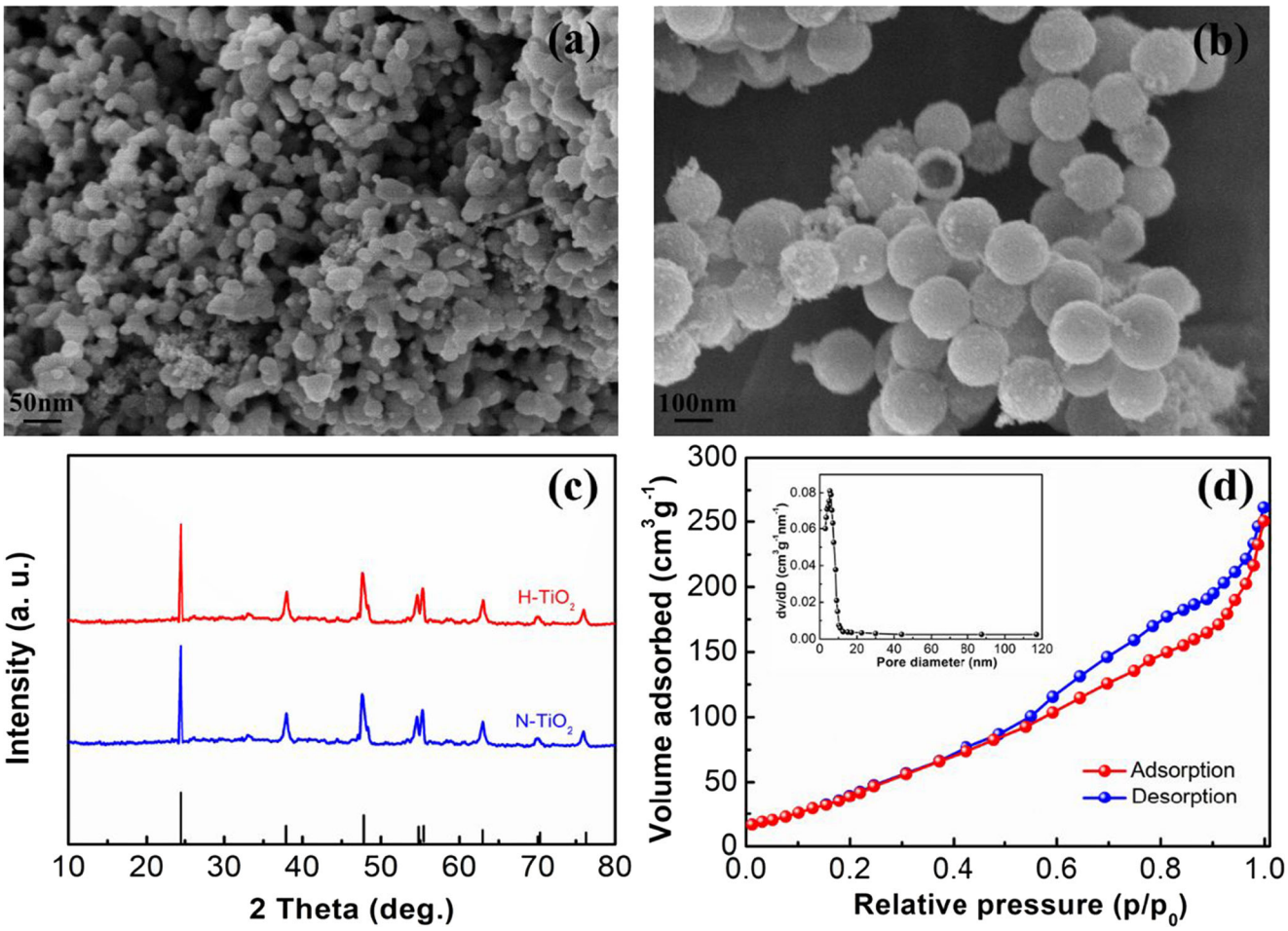

Fig. 2 SEM images of **a** N-TiO_2, **b** H-TiO_2; **c** XRD patterns of H-TiO_2 and N-TiO_2; **d** nitrogen adsorption–desorption isotherms of H-TiO_2, the inset shows the pore size distribution

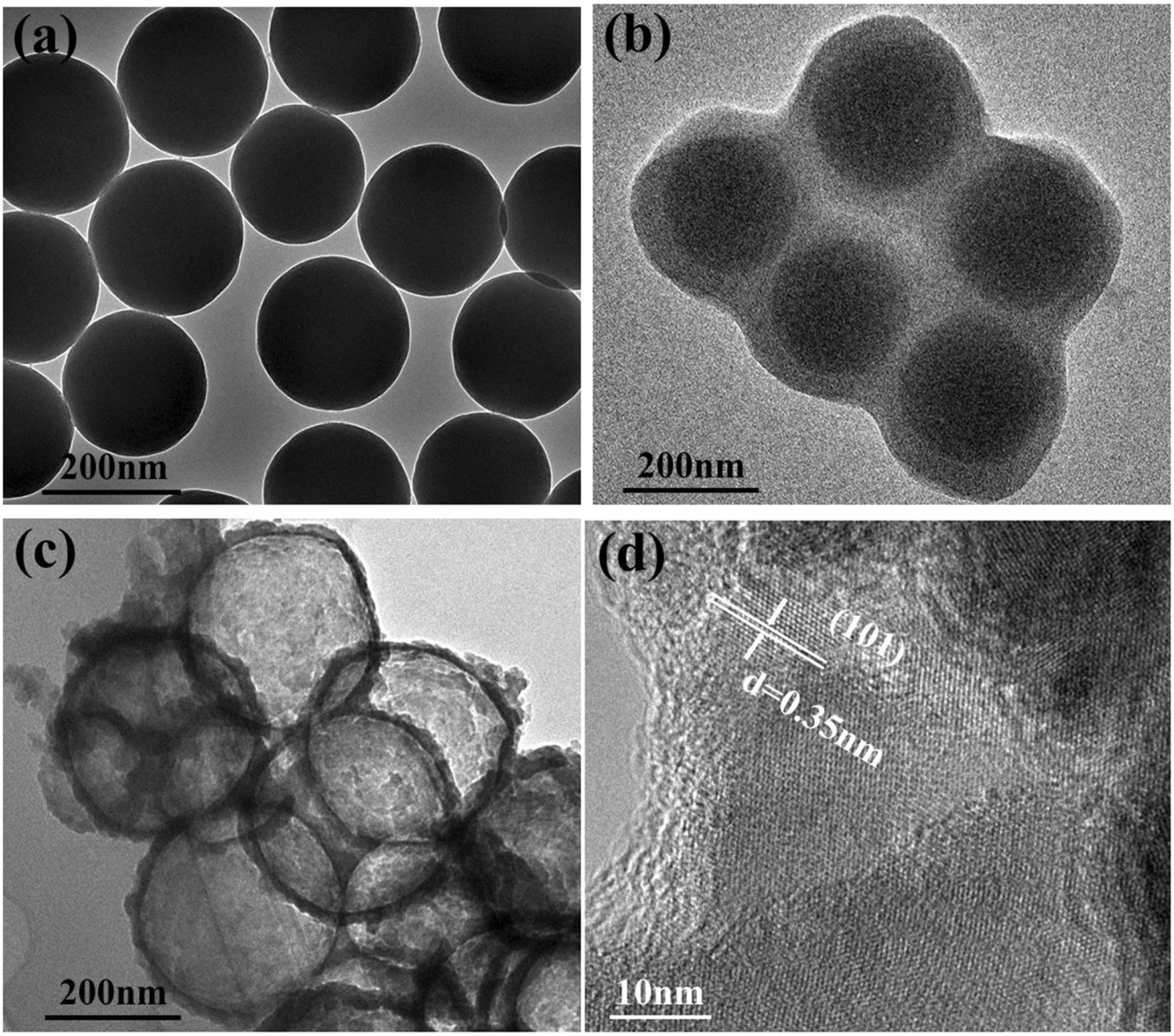

Fig. 3 TEM images of **a** SiO_2, **b** TiO_2@SiO_2, and **c** H-TiO_2; **d** HRTEM image of H-TiO_2

corresponding to the characteristic isotherms of mesoporous materials [11, 22]. The Brunner-Emmett-Teller (BET) specific surface area of the H-TiO_2 yields to be ~225 m^2 g^{-1}. The pore size distribution curve of the H-TiO_2 (inset of Fig. 2d) confirms the existence of mesopores with size distribution centering at ~7.8 nm. It is worth noting that mesopores can further facilitate Li^+ diffusion in the electrodes and shorten the Li^+ and e^- transport length [23].

The H-TiO_2 were evaluated as anode materials for lithium storage properties in LIBs. The electrochemical properties of the H-TiO_2 were investigated by cyclic voltammetry (CV) in the voltage range of 1–3 V vs Li^+/Li. Fig. 4a shows the CV curves of the H-TiO_2 for the first three cycles at scan rate of 0.1 mV s^{-1}. In the first cycle, a couple of current peaks located at 1.68 V and 2.05 V can be observed, corresponding to the insertion and extraction of lithium ions, respectively [24, 25]. In the second cycle, the reduction peak shifted to a higher potential of 1.7 V and the peak current increased slightly, indicating an activation process. Besides, both the reduction and oxidation peaks of the third cycle almost overlap with the second cycle, which implies that the H-TiO_2 exhibits good reversibility of electrochemical reactions.

The charge and discharge curves of the H-TiO_2 at a current density of 0.1 A g^{-1} are shown in Fig. 3b. The first discharge and charge capacities are 289 and 225 mA h g^{-1}, respectively, and the initial coulombic efficiency (CE) was 77.9%; the loss of capacity is caused by the formation of the solid electrolyte interface (SEI) [26, 27]. And the subsequent charge and discharge curves coincide very well, suggesting the excellent electrochemical reversibility of the H-TiO_2. In addition, the

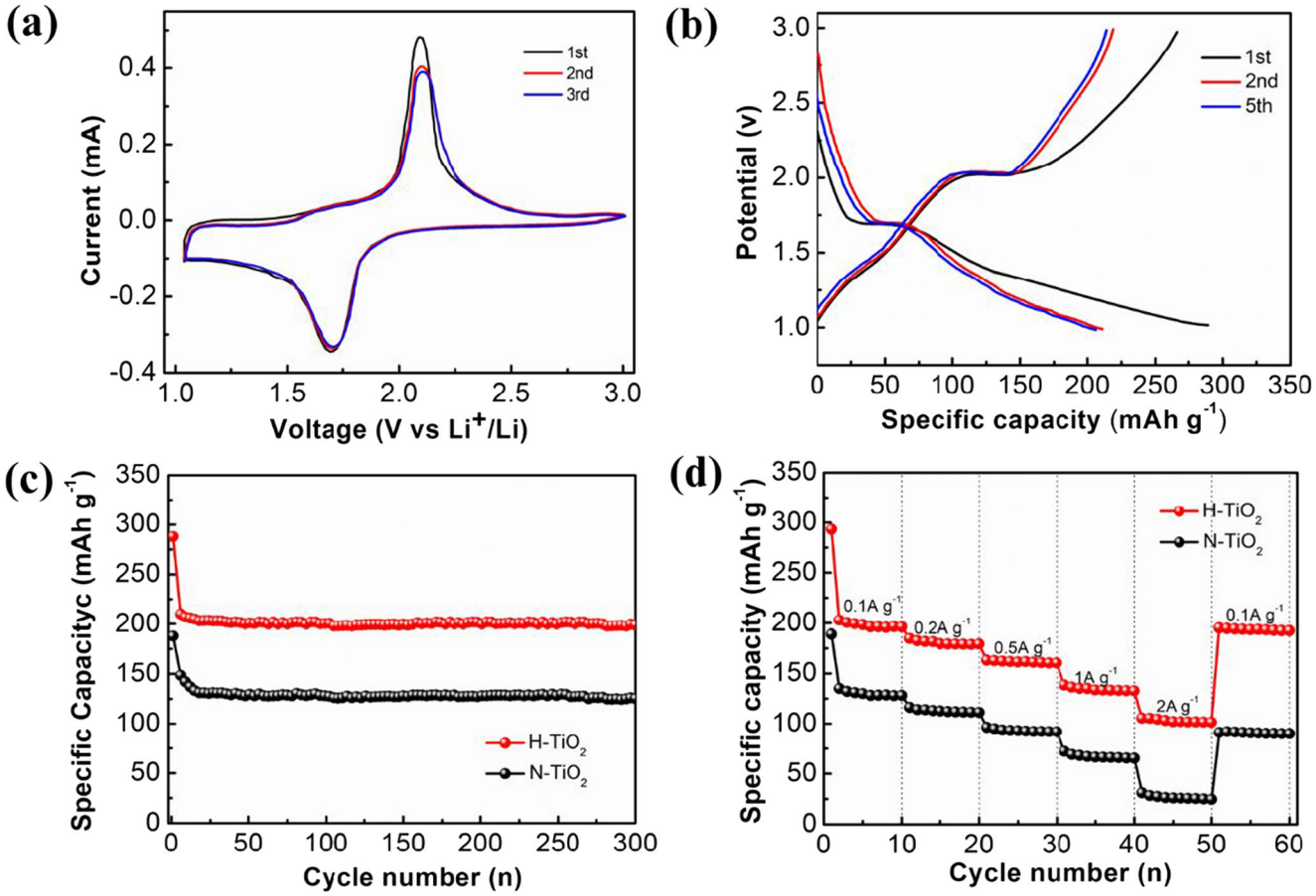

Fig. 4 **a** CV curves of the H-TiO_2 at a scan rate of 0.1 mV s^{-1}; **b** charge and discharge profiles of the H-TiO_2 for the first three cycles at 0.1 A g^{-1}; **c** cycling performance of H-TiO_2 and N-TiO_2 at 0.1 A g^{-1}; **d** rate performance of H-TiO_2 and N-TiO_2 at different current rates from 0.1 to 2 A g^{-1}

curves exhibit two obvious voltage plateaus, 1.7 V for lithium insertion and 2.1 V for lithium extraction, which is in good agreement with the CV curves. Fig. 3c shows the cycling performance of H-TiO_2 and N-TiO_2 at a current rate of 0.1 A g^{-1}. It is obviously observed that the H-TiO_2 exhibits higher discharge capacity of 202 mA h g^{-1}, and there is no rapid capacity decay during the first 15 cycles, which suggesting that H-TiO_2 has a superior cycling performance than N-TiO_2. The cycling performance of the H-TiO_2 electrode is also superior to that of many similar TiO_2-based electrodes, as shown in Table 1. H-TiO_2 and N-TiO_2 were also investigated for rate capability (Fig. 4d). As expected, the H-TiO_2 shows higher discharge capacities of 198, 180, 158, and 135 mA h g^{-1} at current rates of 0.1, 0.2, 0.5, and 1 A g^{-1}, respectively. Even at a very high current rate of 2 A g^{-1}, a capacity of 98 mA h g^{-1} can be still achieved. Compared with N-TiO_2, a discharge capacity of 197 mA h g^{-1} can be recovered when the current rate reduces back to 0.1 A g^{-1}. This demonstrates the superior rate performance and structure stability of H-TiO_2, which could be ascribed to that the hollow structure can shorten the diffusion path for Li^+ and ensure increased contact area between electrodes and electrolyte.

Table 1 Performance comparison of related TiO_2-based materials

Materials	Specific capacity (mA h g^{-1})	Cycles	Current density (A g^{-1})	Reference
TiO_2 nanowires	153	50	0.34	[18]
TiO_2 microboxes	187	300	0.17	[19]
TiO_2 nanofibers	174	50	0.1	[28]
TiO_2 microspheres	132	200	0.34	[29]
N-TiO_2	123	300	0.1	This work
H-TiO_2	196	300	0.1	This work

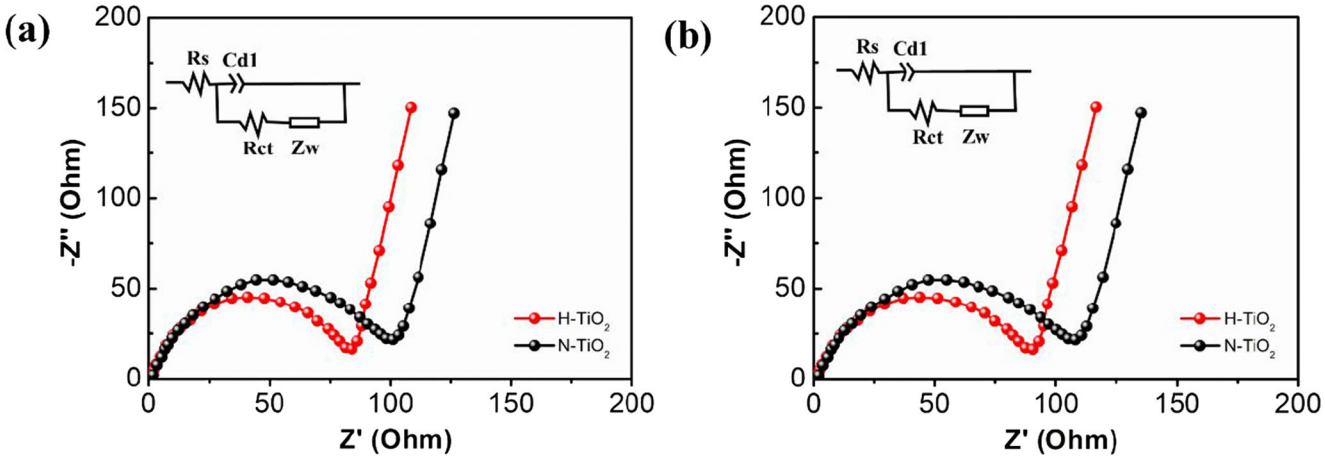

Fig. 5 Nyquist plot of H-TiO_2 and N-TiO_2 **a** before and **b** after 100th cycles (inset is the equivalent circuit model)

The electrochemical impedance spectroscopy was performed to study the resistance property of H-TiO_2 and N-TiO_2. The Nyquist plots display a semicircle in high to medium frequency and a slope line in the low frequency, attributing to charge transfer resistances (*Rct*) and Li-ion diffusion resistances, as shown in Fig. 5 [30, 31]. The corresponding *Rct* values were obtained by measuring the diameter of semicircle that H-TiO_2 and N-TiO_2 before and after cycling 100th show the values of 78 Ω/97 Ω and 83 Ω/112 Ω, respectively. The H-TiO_2 presents lower *Rct* value than N-TiO_2 before and after cycling, indicating better Li-ion transfer ability of H-TiO_2. And the *Rct* values of H-TiO_2 only slightly increase, demonstrating a stable charge/discharge reaction [32, 33]. The basis of lithium storage from the Li-ion diffusion of the two electrodes was investigated by CV measurements at various scan rates ranging from 0.1 to 5 mV s^{-1} (Fig. 6a and b). The linear relationship between peak current density (I_p) and the square root of scan rates is correlated to the corresponding Li-ion diffusion. As can be observed from Fig. 6c, the H-TiO_2 electrode exhibits larger slope than N-TiO_2 electrode, indicating better Li-ion diffusion in the H-TiO_2 electrode. In addition, based on the classical Randles-Sevcik equation, the corresponding Li-ion diffusion coefficient can be calculated [34]:

$$I_p = 2.6 \times 10^5 n^{1.5} A D_{Li}^{0.5} v^{0.5} C$$

where I_p is the peak current density (A g^{-1}), n is the number of reaction electrons in LIBs, A is the electrode area (cm^{-2}), v is the scan rates (V s^{-1}), D_{Li} is the Li-ion diffusion coefficient (cm^2 s^{-1}), and C is the Li-ion concentration (mol ml^{-1}). The corresponding Li-ion diffusion coefficients of H-TiO_2 electrode are larger than N-TiO_2 electrode, which further suggesting the superior Li-ion diffusion property in the H-TiO_2 electrode. This may be attributed to the hollow structure with abundant mesoporous, which can not only provide more channels for Li-ion diffusion but also shorten the transport pathways for Li-ion.

Conclusion

In summary, the TiO_2 hollow nanospheres have been efficiently prepared via a hard-template method. Owning to large specific area and rich mesoporous of the hollow spherical structure, the as-obtained material used as anode for LIBs exhibits high reversible capacity, superior rate capability,

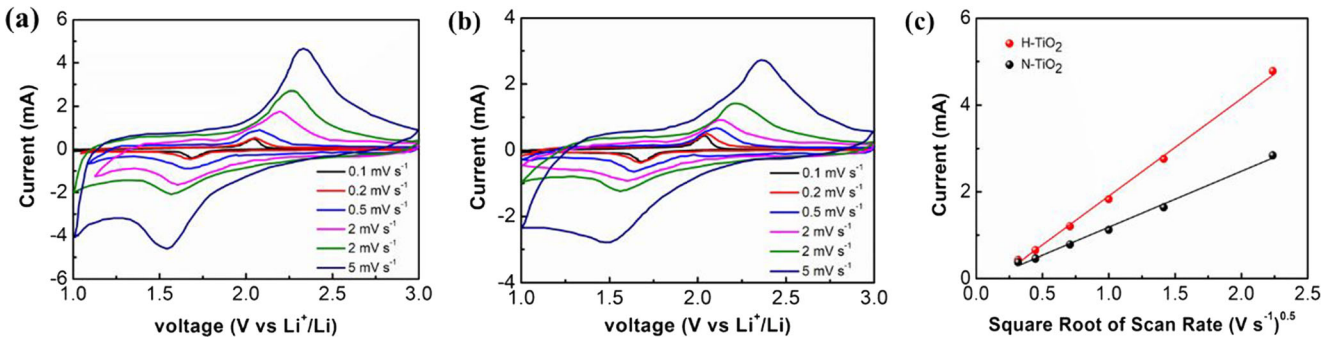

Fig. 6 CV curves of **a** H-TiO_2 and **b** N-TiO_2 at different scan rates; **c** the cathodic reaction versus the square root of scan rates

and excellent long-term cycling stability. The excellent electrochemical performance makes the H-TiO_2 an ideal candidate for high-energy anode materials in LIBs.

Supplementary Information The online version contains supplementary material available at https://doi.org/10.1007/s11581-021-04098-7.

Funding This work is supported by the National Natural Science Foundation of China (61604094).

References

1. Wang ZY, Zhou L, Liu XW (2012) Metal oxide hollow nanostructures for lithium-ion batteries. Adv Mater 24:1903–1911
2. Zheng C, He C, Zhang H, Wang W, Lei X (2014) TiO_2 reduced graphene oxide nanocomposite for high-rate application of lithium ion batteries. Ionics 21:51–583
3. Feng HG, Xie P, Xue SL, Li LW, Hou X, Liu ZY, Wu DJ, Wang LW, Chu PK (2018) Synthesis of three-dimensional porous reduced graphene oxide hydrogel/carbon dots for high-performance supercapacitor. J Electroanal Chem 808:321–328
4. Zhao WC, Li SS, Yao HF, Zhang SQ, Zhang Y, Yang B, Hou JH (2017) Molecular optimization enables over 13% efficiency in organic solar cells. J Am Chem Soc 139:7148–7151
5. Pan HL, Hu YS, Chen LQ (2013) Room-temperature stationary sodium-ion batteries for large-scale electric energy storage. Energy Environ Sci 6:2338–2360
6. Ma DW, Li KM, Pan JH (2020) Ultraviolet-induced interfacial crystallization of uniform nanoporous biphasic TiO_2 spheres for durable lithium-ion battery. ACS Appl Energy Mater 3:4186–4192
7. Ren M, Xu H, Li F, Liu W, Gao C, Su L, Li G, Hei J (2017) Sugarapple-like N-doped TiO_2@carbon core-shell spheres as high-rate and long-life anode materials for lithium-ion batteries. J Power Sources 353:237–244
8. Yan WW, Yuan YF, Xiang JY, Wu Y, Zhang TY, Yin SM, Guo SY (2019) Construction of triple-layered sandwich nanotubes of carbon@mesoporous TiO_2 nanocrystalline@carbon as highperformance anode materials for lithium-ion batteries. Electrochim Acta 312:119–127
9. Zhu C, Xia X, Liu J, Fan Z, Chao D, Zhang H, Fan H (2014) TiO_2 nanotube@SnO_2 nanoflake core–branch arrays for lithium-ion battery anode. Nano Energy 4:105–112
10. Zhao D, Hao Q, Xu C (2016) Nanoporous TiO_2/Co_3O_4 composite as an anode material for lithium-ion batteries. Electrochim Acta 211:83–91
11. Hao Q, Chen L, Xu C (2014) Facile fabrication of a three dimensional cross-linking TiO_2, nanowire network and its long term cycling life for lithium storage. ACS Appl Mater Interfaces 6:10107–10112
12. Wang XB, Wang YY, Yang L, Wang K, Lou XD, Cai BB (2014) Template-free synthesis of homogeneous yolk-shell TiO_2 hierarchical microspheres for high performance lithium ion batteries. J Power Sources 262:72–78
13. Zhu CY, Zhang YN, Yu XH, Dong P, Duan JG, Liu JM, Liu JX, Zhang YJ (2020) Controllable fabrication and Li storage kinetics of one-dimensional spinel $LiMn_2O_4$ positive materials for lithium-ion batteries: an exploration of critical diameter. ChemSusChem 13:801–810
14. Zhang YN, Zhang YJ, Rong J, Wu JH, Dong P, Xu ML, Feng J, Gu CD (2019) Design and controllable synthesis of core-shell nanostructured Ni-P particles with an ionothermal strategy. J Alloys Compd 795:177–186
15. Wang FX, Wang C, Zhao YJ, Liu ZC, Chang Z, Fu LJ, Zhu YS, Wu YP, Zhao DY (2016) A quasi-solid-state Li-ion capacitor based on porous TiO_2 hollow microspheres wrapped with graphene nanosheets. Small 12:6207–6213
16. Wang S, Yu XH, Liu JX, Dong P, Zhang YJ, Zhu CY, Zhan ZL, Zhang YN (2020) Encapsulation of SnO_2 nanoparticles between the hollow TiO_2 nanosphere and the carbon layer as high-performance negative materials for lithium-ion batteries. J Alloys Compd 814:152342–152349
17. Gao C, Peng YQ, Hu LH, Mo LE, Zhang XX, Hayat T, Alsaedi A, Dai SY (2018) A comparative study of the density of surface states in solid and hollow TiO_2 microspheres. Inorg Chem Front 5:2284–2290
18. Tian QH, Song JZ, Zhang ZX, Yang L, Hirano SI (2015) Facile preparation of 3-dimensional interweaved anatase TiO_2 hollow nanowires and its lithium storage properties. Mater Chem Phys 151:66–71
19. Gao XH, Li GR, Xu YY, Hong ZL, Liang CD, Lin Z (2015) TiO_2 microboxes with controlled internal porosity for high-performance lithium storage. Angew Chem Int Ed 54:14331–14335
20. Chen JS, Tan YL, Li CM, Cheah YL, Luan D, Madhavi S, Boey FYC, Archer LA, Lou XW (2010) Constructing hierarchical spheres from large ultrathin anatase TiO_2 nanosheets with nearly 100% exposed (001) facets for fast reversible lithium storage. J Am Chem Soc 132:6124–6130
21. Yu XY, Wu HB, Yu L, Ma FX, Lou XWD (2015) Rutile TiO_2 submicroboxes with superior lithium storage properties. Angew Chem 54:4001–4004
22. Ren H, Yu RB, Wang JY, Jin Q, Yang M, Mao D, Kisailus D, Zhao HJ, Wang D (2014) Multishelled TiO_2 hollow microspheres as anodes with superior reversible capacity for lithium ion batteries. Nano Lett 14:6679–6684
23. Meng R, Hou H, Liu X, Duan J, Liu S (2015) Binder-free combination of graphene nanosheets with TiO_2 nanotube arrays for lithium ion battery anode. J Porous Mater 23:569–575
24. Li C, Zhao M, Sun CN, Jin B, Yang CC, Jiang Q (2018) Surface-amorphized TiO_2 nanoparticles anchored on graphene as anode materials for lithium-ion batteries. J Power Sources 397:162–169
25. Cai Y, Wang HE, Zhao X, Huang F, Wang C, Deng Z, Li Y, Cao GZ, Su BL (2017) Walnut-like porous core/shell TiO_2 with hybridized phases enabling fast and stable lithium storage. ACS Appl Mater Interfaces 9:10652–10663
26. Fang R, Xiao W, Miao C, Mei P, Zhang Y, Yan X, Jiang Y (2019) Enhanced lithium storage performance of core-shell structural Si@TiO_2/NC composite anode via facile sol-gel and in situ N doped carbon coating processes. Electrochim Acta 317:575–582
27. Zhang G, Wu HB, Song T, Paik U, Lou XW (2014) TiO_2 hollow spheres composed of highly crystalline nanocrystals exhibit superior lithium storage properties. Angew Chem Int Ed Engl 53(46):12590–12593
28. Li J, Liu HD, Hu ZL, Chen Y, Ruan HB, Zhang L, Hu R (2016) Facile approach to prepare TiO_2 nanofibers via electrospinning as anode materials for lithium ion batteries. J Mater Sci 27:8682–8687
29. Zhen MM, Li KF, Guo SQ, Li HZ, Shen BX (2021) Template-free construction of hollow TiO_2 microspheres for long-life and high-capacity lithium storage. J Alloys Compd 859:157761–157768

30. Liu H, Li W, Shen D, Zhao D, Wang G (2015) Graphitic carbon conformal coating of mesoporous TiO_2 hollow spheres for high performance lithium ion battery anodes. J Am Chem Soc 137(40): 13161–13166
31. Cai Y, Wang HE, Jin J, Huang SZ, Yu Y, Li Y, Feng SP, Su BL (2015) Hierarchically structured porous TiO_2 spheres constructed by interconnected nanorods as high performance anodes for lithium ion batteries. Chem Eng J 281:844–851
32. Yuan YF, Chen Q, Zhu M, Cai GS, Guo SY (2021) Nano tube-in-tube CNT@void@TiO_2@C with excellent ultrahigh rate capability and long cycling stability for lithium ion storage. J Alloys Compd 851:156795
33. Zheng YQ, Yuan YF, Tong ZW, Yin H, Yin SM, Guo SY (2020) Watermelon-like TiO_2 nanoparticles(P25)@microporous amorphous carbon sphere with excellent rate capability and cycling performance for lithium ion batteries. Nanotechnol 31:215407
34. Li P, Shao LY, Wang PF, Yu HX, Qian SS, Shui M, Long NB, Shu J (2015) Lithium sodium vanadium phosphate and its phase transition as cathode material for lithium ion batteries. Electrochim Acta 180:120–128